

Multifunctional nanoparticle PEG-Ce6-Gd for MRI-guided photodynamic therapy

DAN XU^{1*}, AJU BAIDYA^{1*}, KAI DENG², YU-SHUANG LI¹, BO WU¹ and HAI-BO XU¹

¹Department of Radiology, Zhongnan Hospital of Wuhan University, Wuhan University, Wuhan, Hubei 430071;

²Department of Chemistry, Key Laboratory of Biomedical Polymers of Ministry of Education, Wuhan University, Wuhan, Hubei 430072, P.R. China

Received June 16, 2020; Accepted November 12, 2020

DOI: 10.3892/or.2020.7871

Abstract. Gliomas are one of the most common types of primary brain tumors. Despite recent advances in the combination of surgery, radiotherapy, systemic therapy (chemotherapy, targeted therapy) and supportive therapy in the multimodal treatment of gliomas, the overall prognosis remains poor and the long-term survival rate is low. Thus, it is crucial to develop a novel glioma management method. Due to its relatively non-invasive, selective and repeatable characteristics, photodynamic therapy (PDT) has been investigated for glioma therapy in the past decade, exhibiting higher selectivity and lower side effects compared with those of conventional therapy. However, most of the photosensitizers (PSs) are highly hydrophobic, leading to poor water solubility, rapid degradation with clearance in blood circulation and ultimately, low bioavailability. In the present study, hydrophilic polyethylene glycol (PEG)-chlorin e6 (Ce6) chelated gadolinium ion (Gd³⁺) nanoparticles (PEG-Ce6-Gd NPs) were synthesized via a chelation and self-assembly process. Initially, the cell cytotoxicity of PEG-Ce6-Gd NPs was evaluated with or without laser irradiation. The *in vitro* study demonstrated the lack of toxicity of PEG-Ce6-Gd NPs to tumor cells in the absence of laser irradiation. However, its toxicity was enhanced under laser irradiation. Moreover, the size and weight of brain tumors were significantly decreased in mice with glioma xenografts, which was further confirmed via histological analysis. Subsequently, the results indicated that the PEG-Ce6-Gd NPs had a favorable T₁-weighted contrast performance (0.43 mg ml⁻¹ s⁻¹) and were observed to have significant contrast enhancement at the

tumor site from 0.25 to 1 h post-injection *in vivo*. The favorable MRI, as well as the synergetic photodynamic antitumor effect and antineoplastic ability of PEG-Ce6-Gd NPs was identified. It was suggested that PEG-Ce6-Gd NPs had great potential in the diagnosis and PDT treatment of gliomas, and possibly other cancer types, with prospects of clinical application in the near future.

Introduction

Gliomas are the most common primary tumor in the human brain. According to the World Health Organization (WHO) standards, gliomas are classified into grades I-IV, in which grades I and II are considered low-grade gliomas (LGG), while grades III and IV are high-grade glioma (HGG) (1). Glioblastoma multiforme (GBM), which is also known as WHO IV gliomas, accounts for approximately 57% of all gliomas. Despite surgery, radiation therapy and chemotherapy, the overall prognosis for patients with GBM remains poor, with a median survival of less than 2 years (2). In the past decade, photodynamic therapy (PDT), a minimally invasive treatment method, has been used in glioma treatment. Compared with traditional therapies, PDT has higher selectivity and fewer side effects (3).

PDT is based on the principle of generating cytotoxic reactive oxygen species (ROS) (3,4), which induces cell apoptosis and tissue destruction photosensitizers (PSs) by laser activation (5,6). Recently, PDT has emerged as an effective medical tool for various cancer treatments (7,8) considering its relatively non-invasive, selective and repeatable characteristics (9). Despite numerous advantages, PDT has not yet been accepted for wide clinical practice due to certain limitations associated with PS (10-12). Most of the PSs are highly hydrophobic, which leads to poor water solubility, rapid degradation with clearance in blood circulation and low bioavailability (12). In addition, the clinically available PSs have poor tumor specificity (13), due to their low molecular weight and fast metabolism (14).

Chlorin e6 (Ce6), as one of the most used second generation PS molecules in PDT, has been reported to generate ROS under laser activation, which can effectively damage the structure and function of cancer cells (15). It also has been modified in multiple ways to assemble nanostructures, such as albumin-based nanostructures [PTX (HSA-Ce6-PTX-RGD-1)] (16) and

Correspondence to: Dr Bo Wu or Dr Hai-Bo Xu, Department of Radiology, Zhongnan Hospital of Wuhan University, Wuhan University, 169 Donghu Road, Wuhan, Hubei 430071, P.R. China
E-mail: wubo5317@whu.edu.cn
E-mail: xuhaibo1120@hotmail.com

*Contributed equally

Key words: theranostics, magnetic resonance imaging, photodynamic therapy, photosensitizer, chlorin e6, gadolinium, glioma

peptide-based nanostructures [Fmoc-L-Lys/Ce6 (FCNPs) and CDP/Ce6 (CCNPs)] (17). These nanosystems increase PS uptake of tumor cells via the enhanced permeability and retention (EPR) effect, resulting in the increase in photodynamic therapy efficacy and a decrease in non-specific phototoxicity (18,19). To formulate nanostructure PSs, low molecular weight PSs are modified with polymers or antibodies, or are incorporated into micelles and liposomes (20-23).

MRI is a non-invasive imaging modality and has several advantages over other imaging modalities, as it provides three-dimensional anatomic images with high spatial resolution, which allows for the application of nanomaterials for early and specific cancer detection and therapy (24,25). Among them, gadolinium (III)-based contrast-enhanced MRI is a preferred choice for the clinical diagnosis of gliomas and preoperative localization. The development of the MRI technique has increasingly relied on contrast agents (CAs) to improve the sensitivity (26). Previous studies have revealed that contrast-enhanced MRI-guided photodynamic therapy using a bifunctional polymer conjugate containing an MRI contrast agent and a photosensitizer is effective for tumor imaging and treatment (27-29).

A variety of theranostics based on different nanoplatforms have been reported (4,16,17,28). However, after integrating the imaging contrast agent and therapy function, the general characteristics of reported theranostics are their complex designs and heavy structures, which limits their further application (4). Instead of simply combining imaging contrast agent and photosensitizers, ideal theranostics should be refined in design and demonstrate high efficiency.

Thus, the aim of the present study was to design theranostic agent PEG-Ce6-Gd nanoparticles (PEG-Ce6-Gd NPs) to identify both imaging and therapy functions in gliomas or other cancer types. PEG is a Food and Drug Administration (FDA)-approved hydrophilic polymer without immunogenicity, antigenicity or cytotoxicity (30). PEGylated nanoparticles present high biocompatibility and water solubility, as well as prolonged circulation time and enhanced accumulation in tumor sites via the EPR effect. After covalent binding with Ce6, the hydrophilicity of Ce6 is improved by reacting to PEG-Ce6. The PEG-Ce6 is then bound to the Gd(III) (31) to obtain an MRI contrast agent of PEG-Ce6-Gd. The PEG-Ce6-Gd NPs are then obtained via the self-assembly of PEG-Ce6-Gd monolayer. These simple but powerful PEG-Ce6-Gd NPs can facilitate MRI diagnosis and PDT treatment of gliomas simultaneously, which has great potential in the diagnosis and PDT treatment of gliomas and potentially other cancer types.

Materials and methods

Materials. 1,2-Distearoyl-sn-glycero-3-phosphoethanolamine-N-[methoxy(polyethylene glycol)-2000] (DSPE-PEG2000) was purchased from Shanghai Advanced Vehicle Technology Co., Ltd. Gadolinium (III) acetate tetrahydrate [$\text{Gd}(\text{C}_2\text{H}_3\text{O}_2)_3 \cdot 4\text{H}_2\text{O}$], Ce6, [4,5-Dimethylthiazol-2-yl]-2,5-diphenyltetrazolium bromide (MTT), N,N'-Dicyclohexylcarbodiimide (DCC), N-Hydroxysuccinimide (NHS), Hoechst-33342, N,N-dimethyl formamide (DMF) and anhydrous dimethyl sulfoxide (DMSO) were purchased from Shanghai Chemical Co., Ltd. All the

chemicals were of reagent grade and used without further purification.

The consumables for cell culture and fetal bovine serum (FBS; Scitecher) were purchased from Beijing Dingguo Changsheng Biotechnology Co., Ltd.

The entire experiment lasted for 1 year from synthetic materials PEG-Ce6-Gd NPs to *in vitro* and *in vivo* experiments.

Synthesis and preparation of PEG-Ce6-Gd NPs. For the synthesis of the NPs, 96 mg Ce6 (0.16 mM), 40 mg DCC (0.192 mM) and 22 mg NHS (0.192 mM) were separately added to a three-flask containing anhydrous DMF (50 ml). The mixture was stirred for 2 h in an ice bath. Then, 320 mg PEG-NH₂ (0.16 mM) was added to the mixture and stirred for another 24 h at room temperature. After filtration, NaOH, regulated at pH 8.0, was added directly to the solution at 50°C. Subsequently, 400 mg Gd(AC)₃ was added and the resulting solution was stirred for 48 h to obtain the final product after purification.

NPs were prepared via a self-assembly process. PEG-Ce6-Gd (100 mg) was dissolved thoroughly in 5 ml acetonitrile. DSPE-PEG (25 mg) in 10 ml ultrapure water was added dropwise into the solution of acetonitrile under vigorous stirring. The mixture was then stirred at room temperature for 24 h to remove the acetonitrile via volatilization (32).

Characterization techniques. A Zeta-Sizer Nano ZS [dynamic light scattering (DLS), Malvern Panalytical Ltd.] was used to measure the size of NPs. The morphology was investigated via transmission electron microscopy (TEM) using JEM-100CXII 100 kV (JEOL, Ltd.). UV-vis absorption spectra were measured using a Hitachi U-3900 spectrophotometer. Fourier transform infrared spectra (FTIR) was performed on a Nicolet IS 10 spectrometer (Thermo Fisher Scientific, Inc.) (6,15).

Measurement of ROS generation of PEG-Ce6-Gd NPs. A total of 0.78-100 $\mu\text{g}/\text{ml}$ of PEG-Ce6-Gd NPs were incubated with 40 μM 2',7'-dichlorofluorescein diacetate (DCFH) and irradiated with 630 nm (200 mW/cm^2 for 30 sec). Subsequently, the fluorescence intensity of dichlorofluorescein (DCF) was detected using a fluorescence spectrophotometer (RF-5301pc, Shimadzu) (7,15).

Cell culture. The rat glioma C6 cell line was purchased from Shanghai Fuheng Cell Center, and was cultured in F12K (Shanghai Fuheng Cell Center, Shanghai, China). All of the media were supplemented with 10% FBS and 2% (v/v) streptomycin-penicillin. Cells were maintained in medium in an air atmosphere with 5% CO₂ at 37°C.

Photocytotoxicity. MTT assay was performed to evaluate the photocytotoxicity of PEG-Ce6-Gd NPs in comparison to free Ce6. In two previous studies, cells were incubated with free Ce6 at the same concentrations (0.5 and 1 $\mu\text{g}/\text{ml}$) for 12 and 24 h, and results showed that the cell survival rate was identical, approximately 90 and 80% respectively (6,10). Thus, the cells were incubated with PEG-Ce6-Gd NPs for 12 h in the present study. Briefly, cells were cultured in 96-well microplates at a concentration of 5×10^5 per well for 24 h. Then, the different concentrations of PEG-Ce6-Gd NPs (1.25 $\mu\text{g}/\text{ml}$

was the highest) were added and incubated for 12 h. The cells were washed three times with PBS and each well underwent laser treatment for 12 min in total, and then 100 μ l of fresh culture medium was added in each well before incubation for another 24 h. Subsequently, 20 μ l of MTT (5 mg/ml in PBS) was added in each well and incubated for 4 h. Then, 100 μ l of DMSO was added in each well to dissolve the purple crystal of formazan. Absorbance at 570 nm was measured using a microplate reader to evaluate cellular metabolic activity (reflects the number of viable cells). Cell viability was calculated using the formula: Cell viability (%) = $A_{\text{sample}}/A_{\text{control}} \times 100\%$, where A_{sample} and A_{control} represent the absorbance values for the treated cells and the untreated control cells, respectively. The A_{sample} and A_{control} values were obtained by subtracting the absorbance of DMSO. Data are presented as the mean \pm SD. The replicate number was four (6,7).

T₁-weighted and T₁-mapping images of PEG-Ce6-Gd. The MRI capability of PEG-Ce6-Gd NPs was characterized by their capacity to alter the T₁ relaxation rate (r_1). A clinical MR scanner (3T, Prisma; Siemens, Healthcare Ltd.) was used to measure the relationship between the T₁ relaxation rate and PEG-Ce6-Gd NPs concentration. For MRI measurements, each of the 96-well plates was filled with 150 μ l solution to achieve T₁-weighted and T₁-mapping images. T₁-weighted images were acquired using a sequence with repetition time (TR) as 700 msec, echo time (TE) as 12 msec, slice thickness as 2.0 mm, matrix size as 0.3x0.3x2.0 mm, field of view (FOV) as 120 mm and number of acquisition as 2. T₁-mapping images were acquired using a sequence with TR as 15 msec, TE as 2.7 msec, slice thickness as 2.0 mm, matrix size as 0.2x0.2x2.0 mm, FOV as 160 mm and number of acquisition as 14 (31).

Animals and tumor model. All animals received care in compliance with the guidelines outlined in the Guide for the Care and Use of Laboratory Animals, and the procedures were approved by the Wuhan University of China Animal Care and Use Committee.

All animals received care in compliance with the guidelines outlined in the Guide for the Care and Use of Laboratory Animals, and the procedures were approved by the Wuhan University of China Animal Care and Use Committee. A total of 20 female BALB/c nude mice (age, 6-8 weeks; weight, 16-18 g) were purchased from Beijing Huafukang Bioscience Co., Ltd., and housed under specific pathogen-free conditions (60% relative humidity; 20°C, room temperature) with a 12-h light/dark cycle, provided and maintained with free access to food and water. The animal health and behavior were monitored once a day. If the tumor-bearing mice had a rapid weight loss of >20% or could not eat or drink, they were euthanized by cervical dislocation after anesthesia with 5% isoflurane; the euthanasia was confirmed by checking there was no heart rate. No mice were found dead during the experiment. The treatment experiment lasted for 10 days. For tumor-bearing mice, C6 cells were suspended in fresh culture medium F12K after trypsinization. Then, a density of 2×10^6 C6 glioma cells was subcutaneously injected in the right flank of each mice (31).

In vivo T₁-weighted and T₁-mapping MRI. MRI was performed out on a Siemens Prima 3.0T MRI scanner. Mice

were anesthetized with 5% isoflurane at room temperature and 2% isoflurane was maintained during subsequent scans. Prior to administration of PEG-Ce6-Gd NPs, the pre-contrast images of mice were obtained. Then, the mice were scanned at 15, 30, and 45 min, as well as 1 and 3 h after PEG-Ce6-Gd NPs injection via the tail vein, respectively. T₁-weighted images were acquired using a sequence with TR as 700 msec, TE as 12 msec, slice thickness as 2.0 mm, matrix size as 0.3x0.3x2.0 mm, FOV as 120 mm and number of acquisition as 2. T₁-mapping images were acquired using a sequence with TR as 15 msec, TE as 2.7 msec, slice thickness as 2.0 mm, matrix size as 0.2x0.2x2.0 mm, FOV as 160 mm and number of acquisition as 14. The replicate number was four (31).

Therapeutic studies in vivo. The tumor was left to inoculate for 5-7 days to achieve an average volume of 200 mm³. The anti-tumor effect of PEG-Ce6-Gd NPs was studied under laser irradiation. Mice-bearing subcutaneous tumors were randomly separated into four groups with five mice in each: i) Control group, received PBS injection; ii) PEG-Ce6-Gd NPs group, received PEG-Ce6-Gd NPs injection; iii) laser group, received laser irradiation; and iv) PDT group, received PEG-Ce6-Gd NPs and laser irradiation. The treatment was performed for 10 days. After the first therapy, tumor size was measured every 2 days using an external digital caliper. In addition, every 2 days 200 μ l of PEG-Ce6-Gd NPs (1 mg/ml of free Ce6 equivalent) was intravenously injected via the tail vein into the tumor-bearing mice in groups 2 and 4. In group 3, irradiation was performed with an intensity of 0.80 W/cm² for 10 min. Specifically, in group 4, irradiation was executed after 1 h of injection with an intensity of 0.80 W/cm² for 10 min. Tumor volumes were measured every 2 days of post-treatment and estimated by using the formula: Tumor volume = $1/2 \times a \times b^2$, where 'a' represents the largest tumor diameter and 'b' represents the shortest tumor diameter. This experiment didn't provide other treatments such as ulcer treatment. The replicate number was four (33).

Histological analysis. The mice were sacrificed when the *in vivo* observation was completed. The tumors and major tissues (heart, lung, liver, spleen and kidney) were collected, washed, fixed with a 4% paraformaldehyde solution at 4°C overnight, and embedded in paraffin. Then, 5- μ m sections were obtained and stained using hematoxylin and eosin (H&E) (11,14).

Statistics analysis. Statistical analysis of the results was performed using SPSS 23.0 (IBM Corp.). Data are presented as the mean \pm SD, and the differences among the groups were analyzed with Bonferroni comparison tests following ANOVA. P<0.05 was considered to indicate a statistically significant difference. T₁-mapping images of various concentrations of PEG-Ce6-Gd NPs incubated without cells and with C6 cells via MRI were the data generated for Fig. 5C and D.

Results

Preparation and characterization of PEG-Gd-Ce6 NPs. A flow chart of the whole experiment is presented in Fig. 1. The synthesis and chemical structure of PEG-Ce6-Gd NPs are shown in Fig. 2. The nanoparticle was self-assembled and chelated with Gd ion into Ce6 via a chelating agent Ce6.

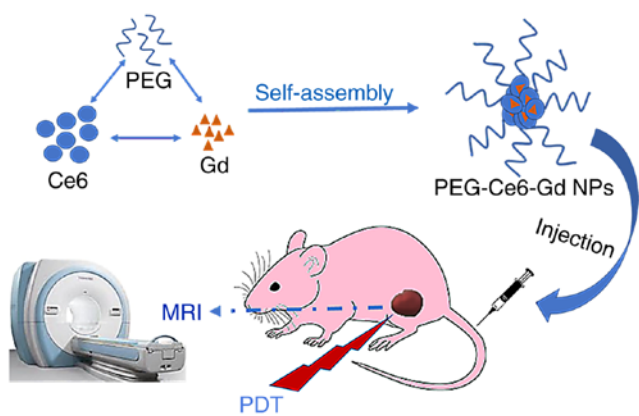


Figure 1. Schematic illustration of PEG-Ce6-Gd NPs for MRI and photodynamic therapy.

The formation of the PEG-Ce6-Gd NPs and PEG-Ce6 was confirmed from the characteristic bands of PEG-Ce6-Gd NPs (in 1110, 2882, and 3422 cm^{-1}) and PEG-Ce6 (in 1110, 2882, and 3430 cm^{-1}) in the FTIR spectra (Fig. 3A). The UV/V is absorption spectra of Ce6 and PEG-Ce6 in the solution displayed a typical porphyrin ring, appearing more intense in the range of 350–450 nm and less intense in the range of 450–700 nm (Fig. 3B). The morphology was evaluated via TEM images. The TEM images of PEG-Ce6-Gd NPs demonstrated a spherical shape within a cyclohexane with a uniform size of about 120 nm in diameter (Fig. 3C). The average hydrodynamic diameter of PEG-Ce6-Gd NPs was measured to be 130 nm using DLS (Fig. 3D), which was large compared with that measured via TEM due to a difference in the measurement mechanism.

ROS generation of PEG-Ce6-Gd NPs. PDT destroys tissues via the production of ROS generated under laser irradiation. Laser irradiation of a sensitizer results in the production of ROS that, in the presence of DCFH, leads to the formation of DCF, a highly fluorescent compound that is easy to detect (34). Thus, the DCF method was used to measure the ROS generation of PEG-Ce6-Gd NPs under 630 nm laser irradiation. As presented in Fig. 4A, the fluorescence intensity of DCF, which was proportional to the ROS production, increased with an increasing concentration of PEG-Ce6-Gd NPs.

Cell viability. C6 cells were incubated with PEG-Ce6-Gd NPs at different concentrations for 12 h in a 96-well plate. The cytotoxicity of the PEG-Ce6-Gd NPs was evaluated separately in the absence and presence of laser irradiation. The results indicated that in the absence of laser irradiation, PEG-Ce6-Gd NPs has a favorable biocompatibility and low cytotoxicity in tumor cells, with >80% cell viability even at the highest concentration (1.25 $\mu\text{g}/\text{ml}$). However, in the presence of laser irradiation, PEG-Ce6-Gd NPs significantly affected cell viability which was reduced to 40% at the highest concentration (1.25 $\mu\text{g}/\text{ml}$). These results indicated the photocytotoxicity effects of PEG-Ce6-Gd NPs on tumor cells under laser irradiation, which suggested that PEG-Ce6-Gd NPs may be promising for the photodynamic therapy in cancer treatment (Fig. 4B).

In vitro MRI of PEG-Ce6-Gd NPs. The MRI contrast efficacy of PEG-Ce6-Gd NPs was evaluated *in vitro* before its application

for cancer treatment. The MRI contrast of the PEG-Ce6-Gd NPs was evaluated by measuring the T_1 relaxation rate (r_1) values as a function of Gd^{3+} concentration. Various concentrations of nanomaterials PEG-Ce6-Gd NPs incubated without cells and with C6 cells were selected as shown in Fig. 5. The data obtained via a 3.0 T Siemens Prisma demonstrated that in T_1 -weighted MRI, the MR signal intensity of PEG-Ce6-Gd NPs can be detected with different enhancement, which increased linearly according to the concentration influencing the T_1 relaxation time. The corresponding image-intensity color mapping also indicated that the PEG-Ce6-Gd NPs significantly shortened the T_1 relaxation time (Fig. 5A and B). Further analysis suggested that the T_1 -weighted MR signal intensity of PEG-Ce6-Gd NPs increased linearly with Gd^{3+} concentration. As shown in Fig. 5C, the r_1 of PEG-Ce6-Gd NPs was 0.43 $\text{mg}/\text{ml}^{-1} \text{ s}^{-1}$ which indicated that PEG-Ce6-Gd NPs had a promising contrast agent property. C6 cells had efficient light uptake after PEG-Ce6-Gd NPs were added and an enhancement on MRI was observed (Fig. 5D).

MRI in subcutaneous mouse models of glioma. To obtain further insight into the MRI contrast property of PEG-Ce6-Gd NPs, *in vivo* MRI was performed on C6 tumor xenograft-bearing nude mice after separate injection of PEG-Ce6-Gd NPs at different time points (pre-injection, 0.25, 0.5, 0.75, 1 and 3 h) via the tail vein. As is evident in Fig. 6, significant enhancement was identified in the T_1 -weighted MR images of the tumors. The tumor site turned markedly bright after 0.25 h of injection of PEG-Ce6-Gd NPs. After 0.5 h of injection, the contrast enhancement in the T_1 -weighted MR image reached a maximum level. After 3 h of injection, the signal intensity decreased gradually with the prolonging time. These results indicated that PEG-Ce6-Gd NPs has a favorable MRI contrast characteristic.

Anti-tumor effect in vivo. To quantitatively evaluate the photodynamic therapeutic efficacy of the nanomaterial, the mice-bearing tumors were separated into four groups: i) Control group, received PBS injection; ii) PEG-Ce6-Gd NPs group, received PEG-Ce6-Gd NPs injection; iii) laser group, received laser irradiation; and iv) PDT group, received PEG-Ce6-Gd NPs injection and laser irradiation. As shown in Fig. 7A and Table SI, the tumors in the PBS group without treatment grew rapidly, which were about 8 times larger compared with the initial tumor volume. Moreover, the tumors of the two groups only irradiated with laser or injected with PEG-Ce6-Gd NPs without laser irradiation were not suppressed, and were about 6 times larger compared with the initial tumor volume. Tumors in PDT treatment using PEG-Ce6-Gd NPs injection under laser irradiation group were significantly suppressed and the tumor volume showed little increase after 10 days of treatment.

After treatment for 10 days, the tumors were removed and weighed. The tumor destruction was obvious in PDT group and the weight of tumor in PDT group was the lightest, indicating that laser irradiation combined with PEG-Ce6-Gd NPs had a cytotoxic effect on the tumor (Fig. 7B and C and Table SII). Following further detailed analysis, it was found that the laser only treatment group or PEG-Ce6-Gd NPs only treatment group demonstrated a tumor inhibition rate of 31 and

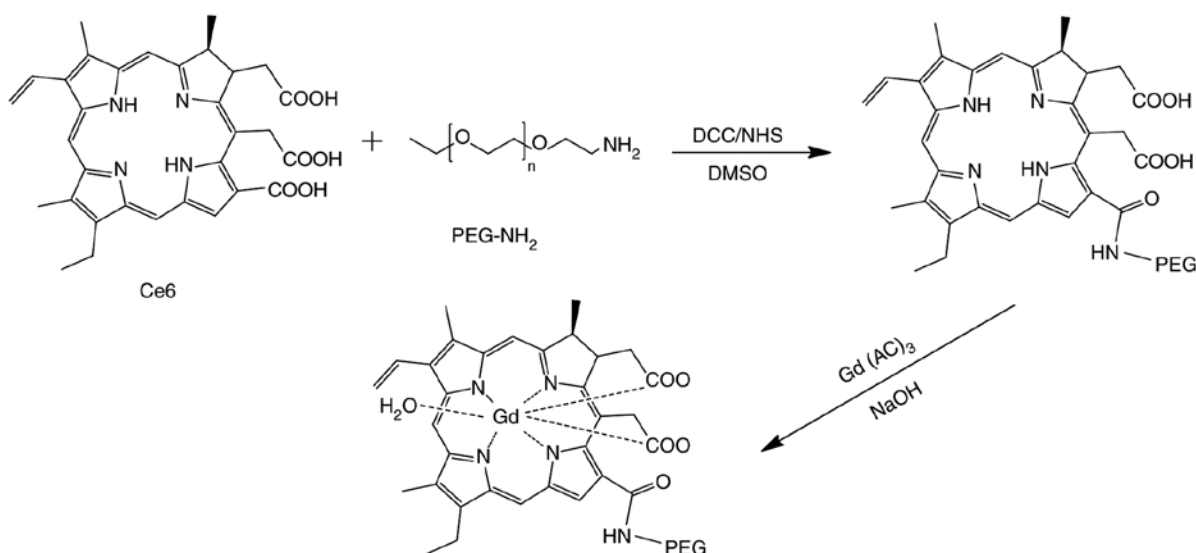


Figure 2. Synthesis Routes of PEG-Ce6-Gd NPs.

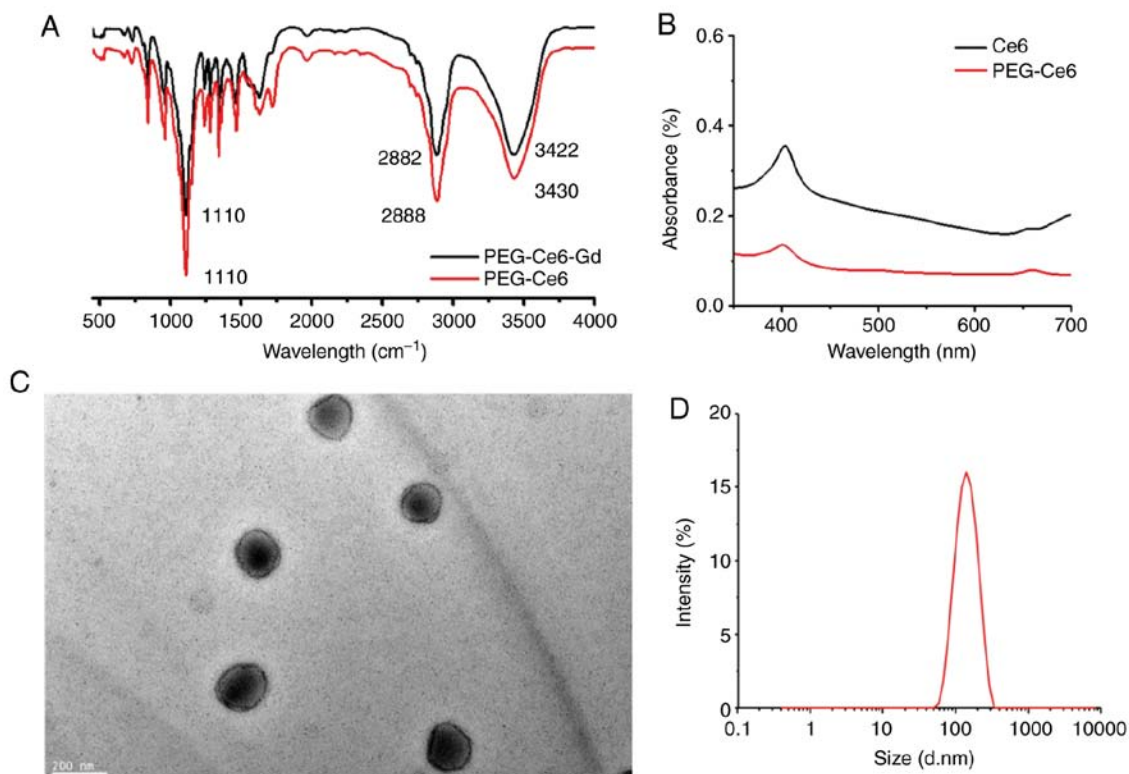


Figure 3. The characterization of PEG-Gd-Ce6 NPs. (A) FTIR spectra of PEG-Ce6-Gd and PEG-Ce6. (B) UV/Vis absorption spectra of PEG-Ce6-Gd and Ce6. (C) TEM images of PEG-Gd-Ce6 NPs (scale bar, 200 nm). (D) The size distribution of PEG-Gd-Ce6 NPs measured using DLS.

60%, respectively. However, the PDT group had a high tumor inhibition rate of 98%. These results demonstrated that the combined laser irradiation and PEG-Ce6-Gd NPs enhanced the anti-tumor ability (Fig. 7D).

Histological analysis. H&E staining identified that the tumor in the PDT group was significantly suppressed compared with that in the control, PEG-Ce6-Gd NPs or laser groups (Fig. 8A and B). In addition, the mice did not have an inflammatory response in major organs, such

as the lung, liver, spleen, kidney and heart, further indicating that PEG-Ce6-Gd NPs at a tested dose had very low toxicity *in vivo* (Fig. 8C). These results demonstrated that PEG-Ce6-Gd NPs can effectively inhibit tumors under laser irradiation with low side effects.

Discussion

The present study reported a type of PEGylated Ce6-Gd NPs, which utilized Ce6 as a binding chelator of paramagnetic metal

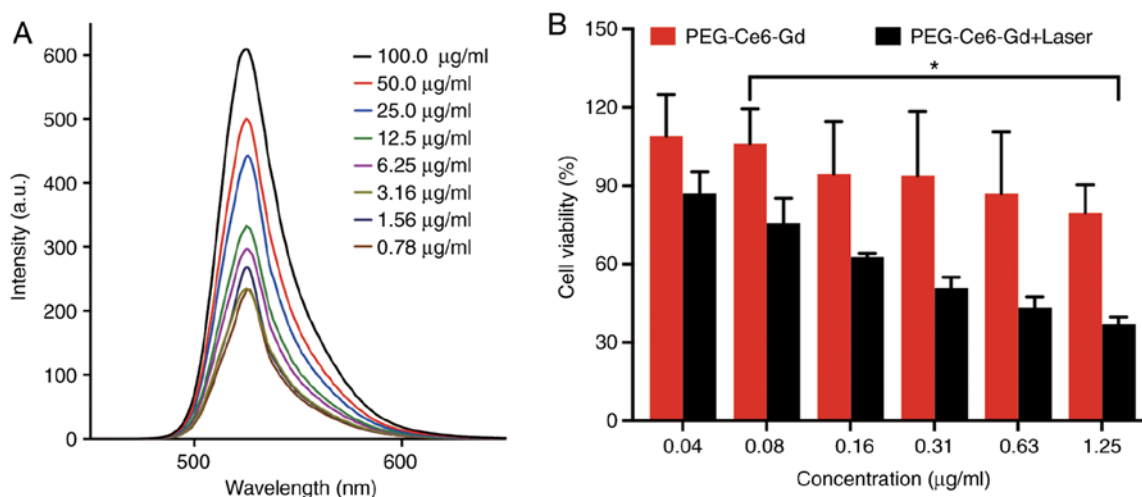


Figure 4. (A) Fluorescence spectrum of DCFH activated with different concentration of PEG-Ce6-Gd NPs under 630 nm laser irradiation. (B) Relative viability of C6 cells incubated with various concentrations of PEG-Ce6-Gd NPs with and without 630 nm laser (0.2 W/cm^2 , 12 min) ($P < 0.05$).

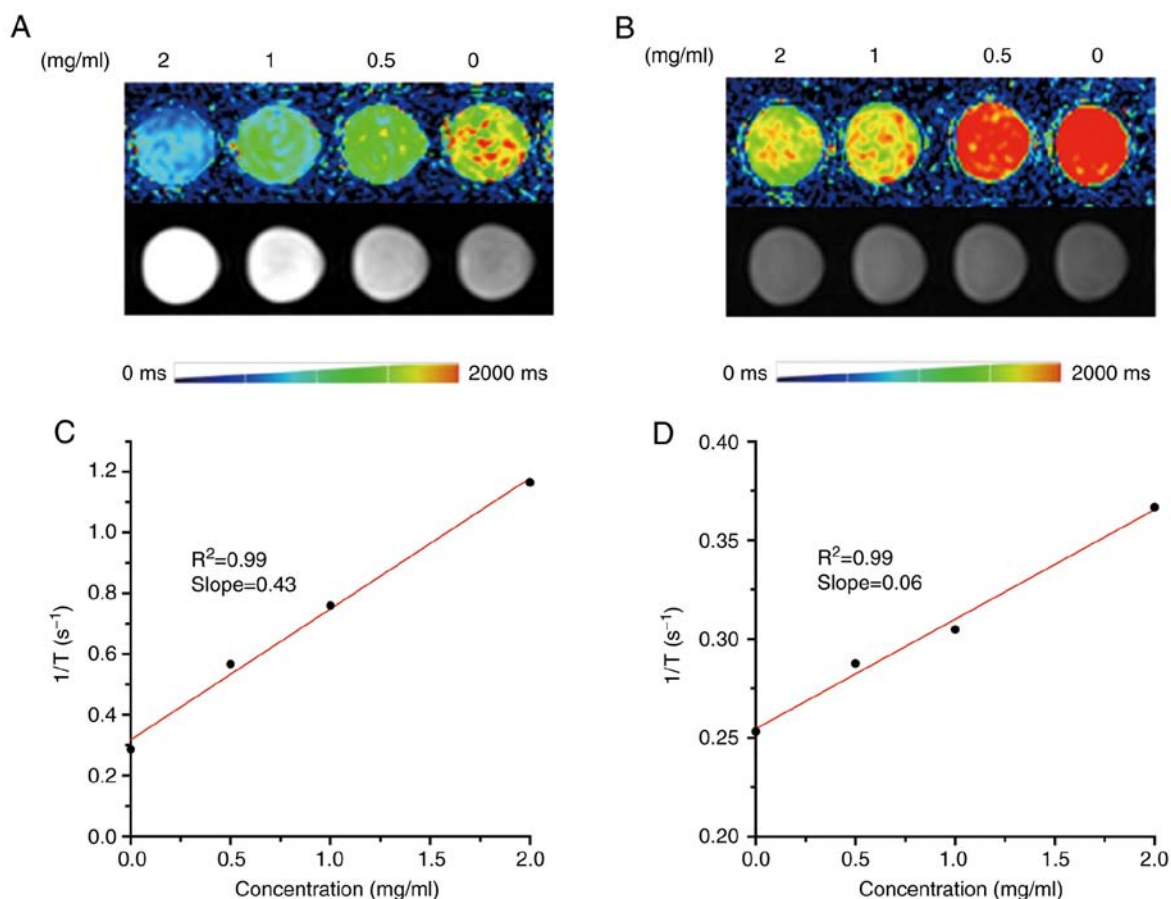


Figure 5. *In vitro* T_1 -weighted MR image of PEG-Ce6-Gd NPs without (A) and with (B) C6 cells incubated at different concentrations and the corresponding pseudo-color image and the intensity bar as a reference scale. T_1 relaxation rate of PEG-Ce6-Gd NPs without (C) and with (D) C6 cells incubated at different concentrations.

ion (Gd^{3+}), and simultaneously retained the photodynamic therapy function of Ce6. The high hydrophobic property of Ce6 enables it to easily form aggregates in aqueous solution, which limits its $^1\text{O}_2$ production. Moreover, hydrophobicity could hinder its solubility in physiological solvents and body fluids, thereby limiting its clinical application (35). PEG is a widely used hydrophilic polymer, which can prolong blood circulation

time and improve biosecurity. In addition, PEGylated NPs accumulate within the tumor stroma via the EPR effect, which improves the therapeutic effect (36). Therefore, in the present study, introducing a hydrophilic group, such as PEG, to improve the hydrophilicity of Ce6 is a possible method for developing advanced theranostics. In addition, the available unpaired electrons in Ce6 were employed to bind Gd^{3+} and served as

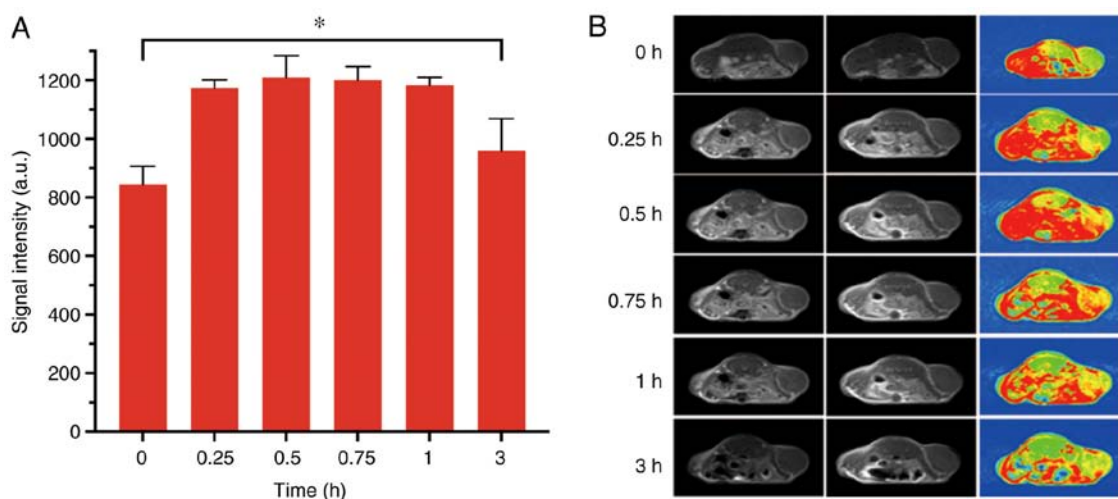


Figure 6. (A) The quantitative analysis of contrast enhanced signals in the tumor region at different time points ($P < 0.05$). (B) *In vivo* T₁-weighted MR images with different concentration of PEG-Ce6-Gd NPs and the corresponding pseudocolor images.

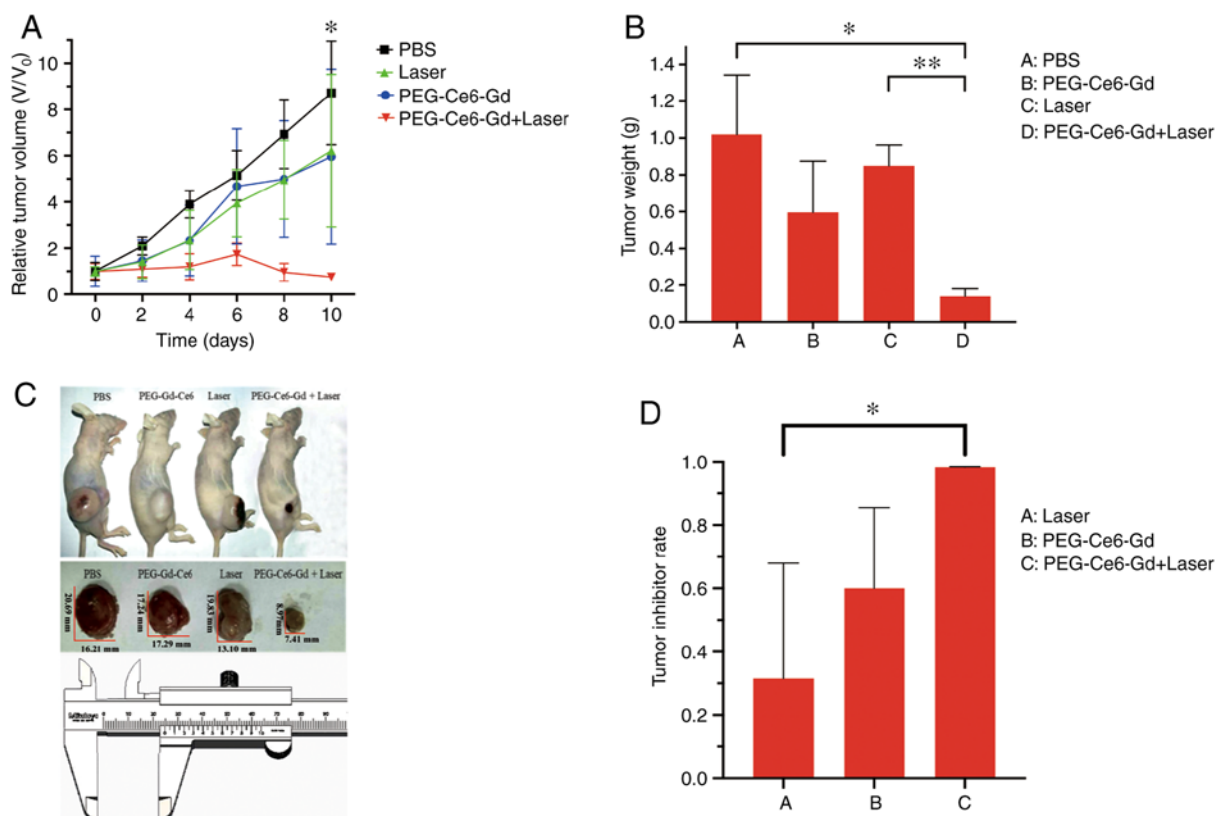


Figure 7. (A) Antitumor effect of PEG-Ce6-Gd NPs on C6 cell xenografts, mean \pm SD. In day 10, PDT groups was significant different from control groups, PEG-Ce6-Gd NPs groups and laser groups. ($P < 0.05$). (B) Tumor weight of mice in different groups ($P < 0.05$, $**P < 0.005$). (C) Photographs of mice with tumor and extracted tumor in various treatment groups (scale bar, 10 mm). (D) The tumor inhibitor rate of different groups after treatment ($P < 0.05$).

a ligands. The PEG-Ce6-Gd NPs exhibited acceptable longitudinal relaxation while maintaining the excellent yields of ROS. These characteristics ensure the imaging contrast effect and PDT therapy of PEG-Ce6-Gd.

Enhanced MRI at different time points can effectively and non-invasively visualize the real-time pharmacokinetics of NPs in mice tumor models. In the present study, the MRI results demonstrated that PEG-Ce6-Gd NPs was relatively prolonged in the blood circulation, and the signal remained

consistent within 0.5-1 h. By contrast, the clinic contrast agent Gd-DOTA was rapidly metabolized within 30 min (37). This difference may be due to the hydrophilicity of PEG, as well as the reduced recognition by liver macrophages (Kupffer cells) and splenic macrophages.

In the present study, the tumors were inhibited to a greater extent with PEG-Ce6-Gd NPs under irradiation. Moreover, PEG-Ce6-Gd NPs had no effect on other healthy tissues. Compared with traditional treatment methods, PDT has its own

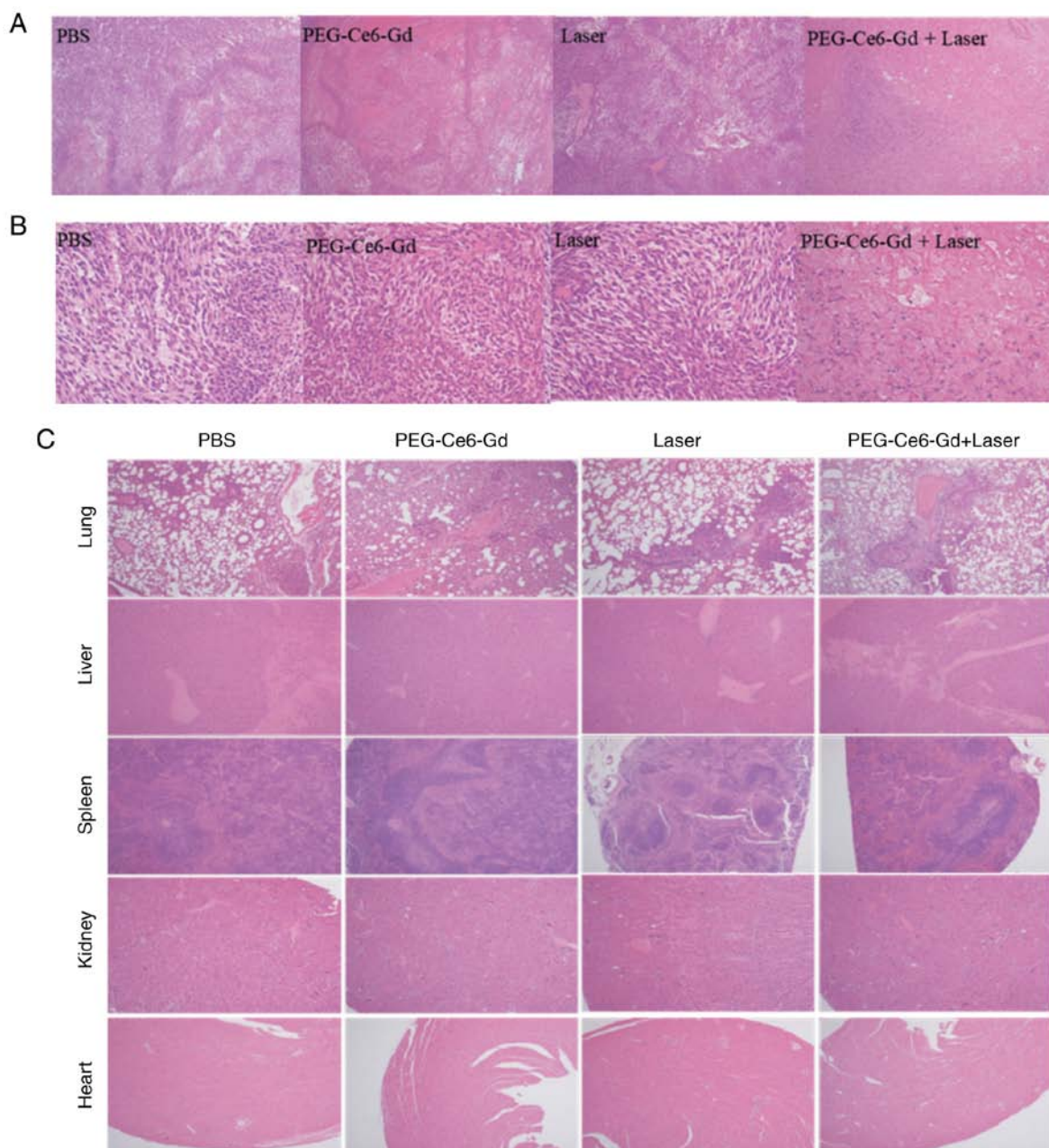


Figure 8. H&E staining of tumor area from the mice in various treatment groups, (A) Magnification, x40, (B) Magnification, x200. (C) Histological analysis of the major organs of mice after different treatments (Magnification, x40). H&E, hematoxylin and eosin.

advantages. Chemotherapy and radiotherapy can respectively induce systemic toxicity and destroy healthy tissues, while PDT itself has no toxic effect on the biological system. PDT also has minimal invasiveness, has repeatability without cumulative toxicity and can be used as an adjunctive therapy following surgical resection, which decreases residual tumor tissue, reduces recurrence rate and improves the quality of life of patients (36).

However, some limitations of this study were first that PEG-Ce6-Gd NPs were not used in the orthotopic glioma model. The typical penetration depth of red light in living tissues used in PDT is only 1-3 mm (36); therefore, PDT cannot treat deep tumors. Second, 5-aminolevulinic acid (ALA), acts as a photosensitizer, has been evaluated clinically for glioma PDT (38). We should compare the therapeutic effect of PEG-Ce6-Gd NPs with 5-ALA in glioma. Thus, future studies

will use PEG-Ce6-Gd NPs in an orthotopic glioma model to observe its therapeutic effect and compare with 5-ALA.

In conclusion, multifunctional NPs (PEG-Ce6-Gd NPs) were synthesized via a self-assembly process, which was designed for cancer diagnosis and treatment. The prepared non-toxic PEG-Ce6-Gd NPs were identified as promising nano-agents for photodynamic therapy and contrast-enhanced MRI diagnosis. The synthesized NPs were able to significantly increase its phototoxicity under laser irradiation, thus inducing death of cancer cell death. *In vitro* and *in vivo* studies demonstrated the beneficial therapeutic efficacy of PEG-Ce6-Gd NPs under laser irradiation. All the observations indicated its potential in clinical PDT cancer treatment. Thus, this novel theranostic agent, PEG-Ce6-Gd NPs, could facilitate diagnosis and PDT treatment of gliomas, and potentially other cancer types.

Acknowledgements

Not applicable.

Funding

This work was financially supported by National Natural Science Foundation of China (grant nos. 81701685 and 81771819) and the National Key Research and Development Program of China (grant no. 2017YFC0108803). The authors from the corporation only provide the technical support and have no financial interest.

Availability of data and materials

The datasets used and/or analyzed during the current study are available from the corresponding author on reasonable request.

Authors' contributions

AB and DX wrote the initial draft of the paper. KD collected and analyzed the data of material characterization, AB, and YS Li collected and analyzed *in vitro* experimental data. AB provided a nude mouse tumor model; AB, and DX provided the MRI scanning for the contrast and the animal; Bo Wu and H-BX conceived the idea of the study and provided the funding. All authors have given approval to the final version of the manuscript.

Ethics approval and consent to participate

Not applicable.

Patient consent for publication

Not applicable.

Competing interests

The authors declare that they have no competing interests, and all authors should confirm its accuracy.

References

- Louis DN, Perry A, Reifenberger G, von Deimling A, Figarella-Branger D, Cavenee WK, Ohgaki H, Wiestler OD, Kleihues P and Ellison DW: The 2016 world health organization classification of tumors of the central nervous system: A summary. *Acta Neuropathol* 131: 803-820, 2016.
- Tan AC, Ashley DM, López GY, Malinzak M, Friedman HS and Khasraw M: Management of glioblastoma: State of the art and future directions. *CA Cancer J Clin* 70: 299-312, 2020.
- Celli JP, Spring BQ, Rizvi I, Evans CL, Samkoe KS, Verma S, Pogue BW and Hasan T: Imaging and photodynamic therapy: Mechanisms, monitoring, and optimization. *Chem Rev* 110: 2795-2838, 2010.
- Bhaumik J, Mittal AK, Banerjee A, Chisti Y and Banerjee UC: Applications of phototheranostic nanoagents in photodynamic therapy. *Nano Res* 8: 1373-1394, 2015.
- Lovell JF, Liu TW, Chen J and Zheng G: Activatable photosensitizers for imaging and therapy. *Chem Rev* 110: 2839-2857, 2010.
- Hou W, Xia F, Alves CS, Qian X, Yang Y and Cui D: MMP2-Targeting and redox-responsive PEGylated chlorin e6 nanoparticles for cancer near-infrared imaging and photodynamic therapy. *ACS Appl Mater Interfaces* 8: 1447-1457, 2016.
- Fan F, Yu Y, Zhong F, Gao M, Sun T, Liu J, Zhang H, Qian H, Tao W and Yang X: Design of tumor acidity-responsive sheddable nanoparticles for fluorescence/magnetic resonance imaging-guided photodynamic therapy. *Theranostics* 7: 1290-1302, 2017.
- Dolmans DE, Fukumura D and Jain RK: Photodynamic therapy for cancer. *Nat Rev Cancer* 3: 380-387, 2003.
- Castano AP, Demidova TN and Hamblin MR: Mechanisms in photodynamic therapy: Part two-cellular signaling, cell metabolism and modes of cell death. *Photodiagnosis Photodyn Ther* 2: 1-23, 2005.
- Liu K, Xing R, Zou Q, Ma G, Möhwald H and Yan X: Simple peptide-tuned self-assembly of photosensitizers towards anti-cancer photodynamic therapy. *Angew Chem Int Ed Engl* 55: 3036-3039, 2016.
- Xing R, Liu K, Jiao T, Zhang N, Ma K, Zhang R, Zou Q, Ma G and Yan X: An injectable self-assembling collagen-gold hybrid hydrogel for combinatorial antitumor photothermal/photodynamic therapy. *Adv Mater* 28: 3669-3676, 2016.
- Liu Y, Ma K, Jiao T, Xing R, Shen G and Yan X: Water-insoluble photosensitizer nanocolloids stabilized by supramolecular interfacial assembly towards photodynamic therapy. *Sci Rep* 7: 42978, 2017.
- Allison RR, Downie GH, Cuenca R, Hu XH, Childs CJ and Sibata CH: Photosensitizers in clinical PDT. *Photodiagnosis Photodyn Ther* 1: 27-42, 2004.
- Vaidya A, Sun Y, Feng Y, Emerson L, Jeong EK and Lu ZR: Contrast-enhanced MRI-guided photodynamic cancer therapy with a pegylated bifunctional polymer conjugate. *Pharm Res* 25: 2002-2011, 2008.
- Yue C, Zhang C, Alfranca G, Yang Y, Jiang X, Yang Y, Pan F, de la Fuente JM and Cui D: Near-infrared light triggered ROS-activated theranostic platform based on Ce6-CPT-UCNPs for simultaneous fluorescence imaging and chemo-photodynamic combined therapy. *Theranostics* 6: 456-469, 2016.
- Chen Q, Wang X, Wang C, Feng L, Li Y and Liu Z: Drug-induced self-assembly of modified albumins as nano-theranostics for tumor-targeted combination therapy. *ACS Nano* 9: 5223-5233, 2015.
- Abbas M, Zou Q, Li S and Yan X: Self-assembled peptide- and protein-based nanomaterials for antitumor photodynamic and photothermal therapy. *Adv Mater* 29, 2017.
- Maeda H, Wu J, Sawa T, Matsumura Y and Hori K: Tumor vascular permeability and the EPR effect in macromolecular therapeutics: A review. *J Control Release* 65: 271-284, 2000.
- Vrouenraets MB, Visser GW, Snow GB and van Dongen GA: Basic principles, applications in oncology and improved selectivity of photodynamic therapy. *Anticancer Res* 23: 505-522, 2003.
- Shiah JG, Sun Y, Peterson CM, Straight RC and Kopecek J: Antitumor activity of N-(2-hydroxypropyl) methacrylamide copolymer-Mesochlorine e6 and adriamycin conjugates in combination treatments. *Clin Cancer Res* 6: 1008-1015, 2000.
- Jiang FN, Liu DJ, Neyndorff H, Chester M, Jiang SY and Levy JG: Photodynamic killing of human squamous cell carcinoma cells using a monoclonal antibody-photosensitizer conjugate. *J Natl Cancer Inst* 83: 1218-1225, 1991.
- van Nostrum CF: Polymeric micelles to deliver photosensitizers for photodynamic therapy. *Adv Drug Deliv Rev* 56: 9-16, 2004.
- Derycke AS and de Witte PA: Liposomes for photodynamic therapy. *Adv Drug Deliv Rev* 56: 17-30, 2004.
- Estelrich J, Sánchez-Martín MJ and Busquets MA: Nanoparticles in magnetic resonance imaging: From simple to dual contrast agents. *Int J Nanomedicine* 10: 1727-1741, 2015.
- Sun BO, Fang Y, Li Z, Chen Z and Xiang J: Advances in the application of nanotechnology in the diagnosis and treatment of gastrointestinal tumors. *Mol Clin Oncol* 3: 274-280, 2015.
- Huang J, Zhong X, Wang L, Yang L and Mao H: Improving the magnetic resonance imaging contrast and detection methods with engineered magnetic nanoparticles. *Theranostics* 2: 86-102, 2012.
- Li G, Slansky A, Dobhal MP, Goswami LN, Graham A, Chen Y, Kanter P, Alberico RA, Sperryak J, Morgan J, *et al*: Chlorophyll-a analogues conjugated with aminobenzyl-DTPA as potential bifunctional agents for magnetic resonance imaging and photodynamic therapy. *Bioconjug Chem* 16: 32-42, 2005.
- Kopelman R, Lee Koo YE, Philbert MA, Moffat B, Reddy GR, Mcconville P, Hall DE, Chenevert TL, Bhojani MS, Buck SM, *et al*: Multifunctional nanoparticle platforms for in vivo MRI enhancement and photodynamic therapy of a rat brain cancer. *J Magn Magn Mater* 293: 404-410, 2005.

29. Gross S, Gilead A, Scherz A, Neeman M and Salomon Y: Monitoring photodynamic therapy of solid tumors online by BOLD-contrast MRI. *Nat Med* 9: 1327-1331, 2003.
30. Larson N and Ghandehari H: Polymeric Conjugates for Drug Delivery. *Chem Mater* 24: 840-853, 2012.
31. Wu B, Li XQ, Huang T, Lu ST, Wan B, Liao RF, Li YS, Baidya A, Long QY and Xu HB: MRI-guided tumor chemo-photodynamic therapy with Gd/Pt bifunctionalized porphyrin. *Biomater Sci* 5: 1746-1750, 2017.
32. Kim KS, Kim J, Kim DH, Hwang HS and Na K: Multifunctional trastuzumab-chlorin e6 conjugate for the treatment of HER2-positive human breast cancer. *Biomater Sci* 6: 1217-1226, 2018.
33. Shi H, Liu Q, Qin X, Wang P and Wang X: Pharmacokinetic study of a novel sonosensitizer chlorin-e6 and its sonodynamic anti-cancer activity in hepatoma-22 tumor-bearing mice. *Biopharm Drug Dispos* 32: 319-332, 2011.
34. Bourré L, Thibaut S, Briffaud A, Rousset N, Eléouet S, Lajat Y and Patrice T: Indirect detection of photosensitizer *ex vivo*. *J Photochem Photobiol B* 67: 23-31, 2002.
35. Lim CK, Heo J, Shin S, Jeong K, Seo YH, Jang WD, Park CR, Park SY, Kim S and Kwon IC: Nanophotosensitizers toward advanced photodynamic therapy of cancer. *Cancer Lett* 334: 176-187, 2013.
36. Lucky SS, Soo KC and Zhang Y: Nanoparticles in photodynamic therapy. *Chem Rev* 115: 1990-2042, 2015.
37. Xu D, Lu ST, Li YS, Baidya A, Mei H, He Y and Wu B: Evaluation of methotrexate-conjugated gadolinium(III) for cancer diagnosis and treatment. *Drug Des Devel Ther* 12: 3301-3309, 2018.
38. Mahmoudi K, Garvey KL, Bouras A, Cramer G, Stepp H, Jesu Raj JG, Bozec D, Busch TM and Hadjipanayis CG: 5-aminolevulinic acid photodynamic therapy for the treatment of high-grade gliomas. *J Neurooncol* 141: 595-607, 2019.



This work is licensed under a Creative Commons Attribution-NonCommercial-NoDerivatives 4.0 International (CC BY-NC-ND 4.0) License.